THE DETECTION OF OH-MASER SATELLITE LINES IN HIGH MASS STAR FORMING REGIONS

by

Derek Felli

A senior thesis submitted to the faculty of

Brigham Young University

in partial fulfillment of the requirements for the degree of

Bachelor of Science

Department of Physics and Astronomy

Brigham Young University

April 2011

BRIGHAM YOUNG UNIVERSITY

DEPARTMENT APPROVAL

of a senior thesis submitted by

Derek Felli

This thesis has been reviewed by the research advisor, research coordinator, and department chair and has been found to be satisfactory.

Date	Victor Migenes, Advisor
Date	Eric Hintz, Research Coordinator
Date	Scott Sommerfeldt, Chair

ABSTRACT

THE DETECTION OF OH-MASER SATELLITE LINES IN HIGH MASS STAR FORMING REGIONS

Derek Felli

Department of Physics and Astronomy

Bachelor of Science

Microwave amplification by stimulated emission of radiation (MASER) originates from molecules which have been pumped to an excited state. Galactic MASER emission originates from dense hot clumps of molecular gas. MASERs are found in star forming regions (SFR), supernova remnants, and late-type stars. There are various very well known MASER species OH^-, H_2O, CH_3OH, SiO, and H_2CO to name some of the most common.

In this work we present the result of studying 41 galactic OH-MASERs using the Very Large Baseline Array (VLBA). Common transitions observed in OH-MASERs are the lines 1612, 1665, 1667, and 1720 MHz. The 1665 and 1667 MHz transitions are more common in SFR and are referred to as "main lines" in the literature. The 1612 and 1720 MHz transitions are common in late-type stars and are known as "satellite lines". Generally 1612 and 1720 MHz lines

are not found in SFR. We studied these four transitions previously mentioned in OH-MASERs, with very high spatial and spectral resolution. We were the first to obtain high resolution observations for 1612 and 1720 MHz transitions in many OH-MASER sources. From our data we determined that the 1720 MHz line strength is correlated of the star formation processes in high-mass and low-mass SFR. Of the 41 sources 5 (11.4%) showed 1612 MHz lines and 10 (22.7%) showed 1720 MHz line. This correlation between satellite line emission and high-mass SFR is helpful in the study of star formation processes.

ACKNOWLEDGMENTS

I would like to thank and acknowledge Dr. Victor Migenes who gave much needed support and help every step of the project. He provided ample help and wisdom in providing help to get through the reduction process of the data. I also would like to acknowledge ORCA in helping fund the research project.

Contents

List of Figures

Chapter 1

Introduction

1.1 Star Forming Regions

Star forming regions (SFR) represent the births of enormous hydrogen fusing entities that will stabilize and self-sustain for long periods of time. A low-mass star typically will live for 10 billion years and a high-mass star for 100 million years. As viewed from our perspective on earth we only can catch a glimpse on the life time of these objects.

A proto-star[1] is a forth-coming star that has not started fusing hydrogen in its core. When Hydrogen fusion starts it becomes classified a main sequence star in the Hertzsprung-Russell (HR) diagram. In the early stages of the proto-star model huge clouds of dust and gas begin to collect to a central location due to some disturbance in the medium. The higher concentration of centrally located dust and gas has an ever increasing gravitational pull on its surrounding and begins to attract more and more matter. Soon after, the in-falling gas and dust will flatten into a disk shape around the proto-star to conserve angular momentum. In these circumstances the

[1] Shu [1]

formation of gas clumps emit radiation named microwave amplification by stimulated emission of radiation (MASER) which is a useful tool to probe the region for certain phenomena. Optical studies prove fruitless because of high content of gas and dust causing obscuration.

We take a look into the microwave emission from SFR to learn about the process of star formation. SFR involve anywhere between 5 and 100 solar masses of gas and dust that obscure the surrounding region. This dust obscures mainly in the optical and prevents many studies from taking place on developing stars. Because microwave wavelengths are not obscured or absorbed in these regions they make the study of forming stars possible. MASER is a strong emission of microwaves that can originate from SFR. MASERs have helped us to "see" deep into the clouded regions in the Universe where we cannot see with visible light.

Our research complements the results of other radio emission detections from SFRs. We observed SFR in our galaxy so we can better understand our galaxy and may be able to project our findings onto other galaxies. This is the first time high spatial and spectral resolution measurements have been taken on some of the known galactic MASER sources. We attempt to further our understanding of the characteristics of high-mass SFR and low-mass SFR through the study of MASERs. We also use this data to improve the current limitations of classifying high-mass and low-mass SFR.

1.2 OH MASERs in the galaxy

1.2.1 What is a MASER

MASER[2] emission in astrophysical settings is a phenomenon where molecules under given conditions emit microwaves radiation. These MASERs come from large clouds called clumps or spots because they appear in such a way in maps. Some clumps are as big as our solar system. These molecules in the cloud are pumped into an excited state having more energy than a ground state. This energy may come from an electron in a higher energy level, rotational energy of the molecule, or vibrational energy of the molecule. The actual source of energy pumping is unknown, but it is believed to come from nearby stars as IR photons for some MASER sources. With this pumping of energy, the electrons in these molecules reach a population inversion where over half of all the electrons are in an excited state. This happens at temperatures around 200 K. An imbalance like a passing photon of similar $\triangle E$ will cause stimulated emission. Stimulated emission is a molecule emitting its energy by a passing photon that has the same energy difference as the energy of the molecule in an excited state from being in the ground state. Albert Einstein showed that a photon has equal probability to cause stimulated emission as it does to be absorb by an atom in the ground state. With more molecules in higher states than ground states, more stimulated emission occurs than absorption. This causes amplification of a photon with energy equal to that of the molecular transition causing a coherent beam to be emitted by the MASER. Microwave radiation is amplified in these hot molecular clouds since many molecules have transitions equal to the energy of photons at the microwave frequency range. These MASERs, being strong emitters of microwave radiation, make great candidates to study the dusty and gaseous environments in SFR.

[2]Caswell [2]

1.2.2 Where MASERs occur

Some astrophysical settings for MASER emission are regions near forming stars, super nova remnants, and late-type stars. The fact that they occur near forming stars and are very intense makes them very important for studying SFR. Recall that dust obscures other wavelength studies. They are usually found in the accreting disk around young stellar objects or in the outflow. Mapping MASER emission can be use identify the central area where the forming star can be found.

MASER emission disappears before the main sequence life of a star begins and they reappear in the latter stages of stellar evolution. Typically the main lines are found in SFR, and the satellite lines are typically found in late-type stars. Late-type stars differ from forming stars in the sense that they are more hot and luminous, and not immediately obscured by dust.

1.2.3 What is the Importance of MASERs in Understanding Star Forming Regions

Detections of MASERs at specific frequencies allows us to study forming stars. The detection lines will be centered at a specific frequency that is red or blue shifted at a common emission line of the laboratory molecules, i.e., OH^-, H_2O, CH_3OH, SiO, and H_2CO. This information is used to determine the composition and velocity of clumps emitting MASER radiation. The radial velocities can help us determine the kinematical condition of the medium like how matter is accreting around the protostar, how fast it is moving, and estimate of the mass of the central object. The emission can also indicate proper motion of outflows from the central portion of the protostar.

Through the presence of magnetic fields splitting of the hyperfine components of the molecule, the magnetic field strength is determined. Knowing the proper motion, velocities, magnetic field strength, and mass of central object are important parameters that star forming models take into account so that we can understand star formation processes [3].

1.2.4 OH-MASER emission of the OH 1612, 1665, 1667, and 1720 MHz lines

We take a look into MASERs stemming from the Hydroxyl molecule, i.e., the OH^- ion, we find that something unusual happens in SFR. The MASER emission from the OH^- molecule has 4 major transitions in the radio range of the spectrum: 1612, 1665, 1667, and 1720 MHz see Fig 1.1. The 1665 and 1667 MHz lines are called main lines because they were the first to be observed and appeared much stronger. The 1612 and 1720 MHz lines are called satellite lines because they are observed on the edges of the main line and were historically detected after the main lines. These transitions occur when an electron in an OH^- molecule absorbs some amount of energy from a photon and the energy is reemitted as a photon. The energy emitted can be used to determine the frequency of the photon

$$E = h\nu. \tag{1.1}$$

Where E is energy, h is Plank's constant and ν is the frequency. By this we know the energies required to excite these transitions. The main lines are more commonly observed in SFR while the satellite lines are more commonly observed in late type stars. The main lines and the satellite lines are from rotational transitions in the OH molecule. Generally satellite lines are not found in SFR. Caswell [4] confirmed

Figure 1.1 The hyperfine splitting of the OH^- molecule. The horizontal red arrows represent an electron falling from a certain energy level when emitting a photon with the frequency indicated

that these are rare finding in SFR. It is of great interest to MASER physics and star formation processes to discover why these lines, 1612 and 1720 MHz, act in such a way. The rare cases where satellite lines appear in SFR provide physical situations we undertake to understand.

1.3 Summary

In this paper we discuss the use of the Very Large Baseline Array (VLBA) and interferometry techniques used to achieve high resolution observations. We reduced VLBA data to look for the satellite lines (1612 and 1720 MHz). These appeared in 14 of the 41 OH-MASERs we observed. The reason why these lines appear is uncertain. Star forming regions must have specific conditions for the satellite lines to occur. Satellite lines are not normally identified with SFR and are considered rare. The results of the observation provide evidence these special conditions occur in high-mass SFR and not in low-mass SFR. Perhaps high-mass SFR provide the photons

necessary to provide the conditions for the four transitions while low-mass SFR only provide for the main lines. As seen in the results of the study, mainly MASERs in high-mass SFR have satellite lines and MASERs from low-mass SFR did not. We ask ourselves why these special conditions inducing the OH-MASER satellite lines are occurring in high-mass SFR and not in low-mass SFR.

Others have done single dish observations. Fish [3] stated, "Over a quarter century has passed since the first OH maser source was observed with very long baseline interferometry (VLBI) resolution by Reid et al. [5]. Since then, only a few more interstellar groundstate OH maser sources have been observed at VLBI resolution (Haschick et al. [6]; Zheng [7]; Slysh et al. 2001b [8], 2002a [9])." Caswell [4] has done VLBI high resolution observations on southern sky MASERs. He found that 1/6 of the SFR with 1665 MHz transition also had 1720 MHz. He agrees that the 1720 MHz transition is mainly associated with super nova remnants and is considered rare in SFR. Our observations supplement these few VLBI observations that have been done on OH-MASERs for studying SFR.

Chapter 2

Interferometric Methods and Data Reduction

Interferometry[1] is the technique that combines the signal of two or more radio antennas in a coherent manner. This is done by combining the radio waves in phase for each antenna in constructive interference. This is possible because light is an oscillatory electromagnetic wave. First, radio dishes need to point at the same object at the same time in order to observe. The location of the telescopes must be known accurately to successfully combine the light signals in phase, along with the time and frequency standard must be kept at each antenna. To add the light in phase we calculate difference in path lengths the light travels to each radio dish.

Each pair of radio dishes can have its signal combined and contribute to the reconstruction of the plane wave arriving from the source. This fills the UV-plane or the planar area we observe at some depth in the sky, so that the intensity and distribution of the emission can be mapped. Baselines are distances between radio dishes. Since we are working with 17.4 and 18.6 centimeter wavelengths, knowing the telescopes

[1]Information in this section mainly came from Thompson [10], Spencer [11], and Anderson [12].

location within a couple of centimeters is necessary. Large baselines contribute to the spatial resolution obtained from doing interferometry. Each satellite forms a baseline to every other satellite in the array. The longest baseline determines the resolution.

$$R = 1.22 * \lambda / D. \tag{2.1}$$

While large baselines allow for high spatial resolution, short baselines contribute to the sensitivity of the observations and help fill the inner UV-plane. As the earth rotates during the integration (observing) time of the frequency sampling all the baselines rotate in an ellipse with respect to the source. Using the earth's rotation allowed for high quality maps of the radio signal to be reconstructed. The VLBA having 45 baselines does a tremendous job in reconstructing the radio plane wave. where the number of radio dishes is ten (n=10) and the number of baselines is given by $(n * (n-1)/2)$ (45 for the VLBA) and adds to the overall signal to reconstruct the original plane-wave.

2.1 Very Long Baseline Array

The Very Long Baseline Array (VLBA) stretches across the U.S. consisting of 10 large satellite dishes of 25 meter diameter. The largest of these baselines is 8611 km. By using interferometric techniques, the radiation that is detected at every dish is cross correlated and adds to the overall signal we wish to observe. The location of the VLBA radio dishes are at the following locations: St. Croix,VI; Mauna Kea, HI; North Liberty, IA; Ft Davis, TX; Los Alamos, NM; Pie Town, NM; Kitt Peak, AZ; Owens Valley, CA; Brewster, WA; Hancook, NH. The VLBA's largest baseline (8611km St. Croix,VI to Mauna Kea, HI) gave us a minimum resolving angle of 0.00510 arcsec and 0.05370 arcsec using Eq. (2.1) for sampling at 1720 and 1612 MHz respectively. This made it possible to resolve many of the sources we observed

Figure 2.1 The VLBA locations

which would not have been possible otherwise [3]. The VLBA instrument provided us with very high resolution spectra and high spatial resolution of our sources.

In January 2001 we sampled 41 sources with the VLBA to obtain high spatial and spectral resolution observations. These sources were known SFR some of which had OH MASER emission previously detected at other spatial resolutions. We sampled with a band width of 250 kHz over 256 channels. We observed at 1612 and 1720 MHz, known transitions of the OH molecule. Choosing the VLBA allowed us to ideally study OH MASER emission because of their compact nature in SFR and the high resolution was helpful in getting detections of OH-MASER emission at the frequencies sampled.

2.2 Data Reduction in Astronomical Image Processing System (AIPS)

The data reduction was completed with the Astronomical Image Processing System (AIPS). The program AIPS is designed to take radio data and perform certain tasks to calibrate and produce plots so that the data can be analyzed in a number of different ways. It does this by running commands called tasks, which take parameters to create calibration tables that affect the data when called upon. AIPS has certain features/tasks available for VLBA data. The data was obtained in FITS format from NRAO as a preferred formatting for AIPS. The data is public and can be obtained from the NRAO website using the Data Vault http://archive.cv.nrao.edu/ searching under the project name BM0132.

The reduction steps for VLBA data should be referenced in the AIPS recipe book which has a full explanation of the standard reduction. Here the order and task and certain parameters used is noted, but if you are not going to be doing the reduction or interested in what we did, skip to the next section Results.

To start out we ran the task FITLD to load the data in AIPS. We then ran INDXR to make a file with a time stamp on all the data to sort it properly. We then ran the FXPOL to fix the polarizations with the data. The data was sampled at two polarizations: left hand circular polarized light and right hand circular polarized light for possible future work and are not used analytically in this work. We combined the light polarizations which is sufficient for the extent of this work. We split the grouped files in half using UVCOP so that AIPS would accept the number of files in each group of files. We then used ANTAB to read in the amplitude calibration information into AIPS.

Next we used APCAL Task to generate an amplitude calibration solution (SN) table. CLCAL was used to smooth the SN table and create a calibration (CL) table. We ran CLCAL on all sources meaning for each assigned FREQID. Then, DTSUM provided a summary of the contents of the dataset to get the integration time.

Next FRING was used to fringe fit data. This was used with CTA102 as the calibrator source. NRAO512, BLLAC, CTA102, 2005+403, and 2007+777 were possible candidates for calibrating sources with bandpass, but CTA102 showed the smoothest bandpass curve to apply to all the sources, with BPASS CTA102 was also used for amplitude and phase calibration. With TACOP, the task to copy tables and other extension files, we put the SN table for CTA102 in both group files. Next we had to run CLCAL with CTA102 as the calibrator source for each of the sources to smooth the calibration solutions. We needed to use the SN table created from the FRING task and had to modify the FREQID in each file (using TABED) to match the FREQID of the source to be calibrated.

The task BPASS to generate a bandpass (BP) table was used for phase calibration with CTA102 as the calibrator source with the CL table for CTA102. TABED was used to make a BP table for sources with a corresponding FREQID. Next, each source underwent the tasks FRING and CLCAL having the source being its own calibrator source with respective CL tables and new SN. We did the exhaustive baseline search to put out as much data as possible. Under the DPARM parameters: we used no. bl combo. We did delay win (nsec). We used 6.8157 for integration time. And we did not average in frequency.

Task SETJY was used to enter source info. into source (SU) table. We entered the SYSVEL and RESTFREQ in LSR for each source. The CVEL task was used to

shift spectral line data a given velocity. This puts each source to a separate file and the old index tables were destroyed, and INDXR was ran for each file for a new index table. Finally the calibration is complete.

Using AIPS we graphed the data with the task POSSM. Normal noise level was 0.1 Jy. Detections around 0.2 Jy above the noise were considered for detection. For weak source then did certain tests such as plotting the data amplitudes vs. time and the amplitude vs. UV to determine if the detection was real. We also compared the spectrum with all baselines with spectrum with data that had long baselines subtracted out. This increases the sensitivity and subtract out noise that sometimes is significant in large baselines.

Chapter 3

Results: Detections of the 1612 and 1720 MHz Lines

We present the following results. Satellite line transitions, being observed in SFR are rare in the first place and did occur in 14 of the 41 sources observed (31.8%) see Table 3.1. Of the 41 sources 5 (11.4%) showed 1612 MHz emission and 10 (22.7%) showed 1720 MHz emission coming from the OH molecule. In our plots Fig. 3.5 the horizontal axis is the local standard of rest (LSR) velocity. The vertical axis is in Janskys (1Jy=$1 * 10^{-26}$W m^{-1} Hz^{-1})

W3OH was the only emitter in our sample to exhibit both 1612 and 1720 MHz transitions and in both circular polarizations. The 1720 MHz emission in RR polarization had two main features see Fig 3.4 . The first was 6 Jansky's above the noise. The second feature was 8.7 Janskys above the noise. The 1720 LL polarization also had two main features. The first was 7.5 Jansky's above the noise . The second feature was 2.3 Janskys above the noise. These features in different polarization were in the same corresponding LSR velocity. W3OH had a 1612 MHz feature 15 Jys above

the noise in LL polarization and 1612 MHz feature 9.8 Jys above the noise in RR polarization 3.3. These LSR velocities also corresponded.

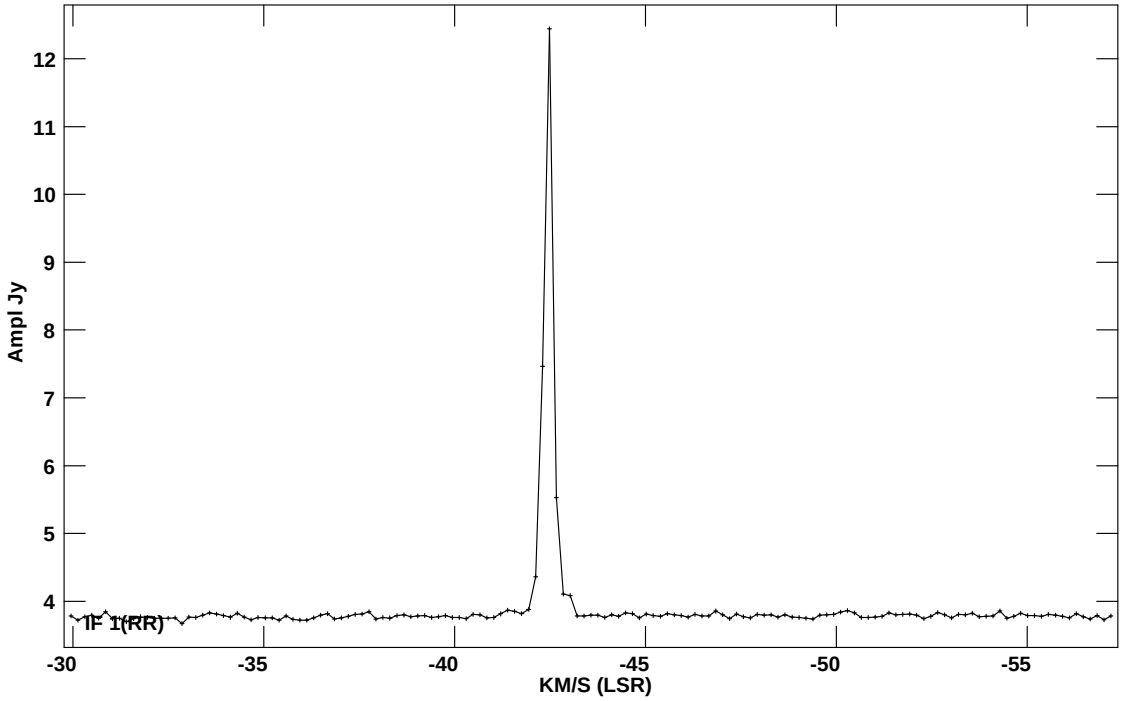

Figure 3.1 MASER detection at 1612 MHz of W3OH in RR polarization.

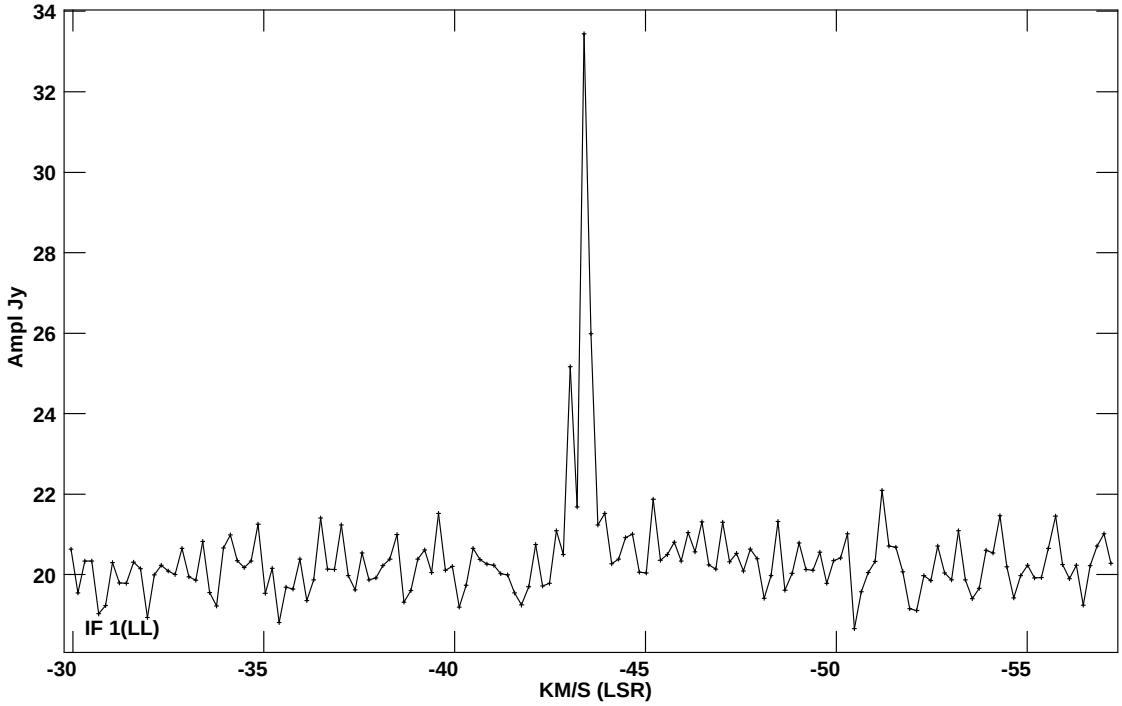

Figure 3.2 MASER detection at 1612 MHz of W3OH in LL polarization.

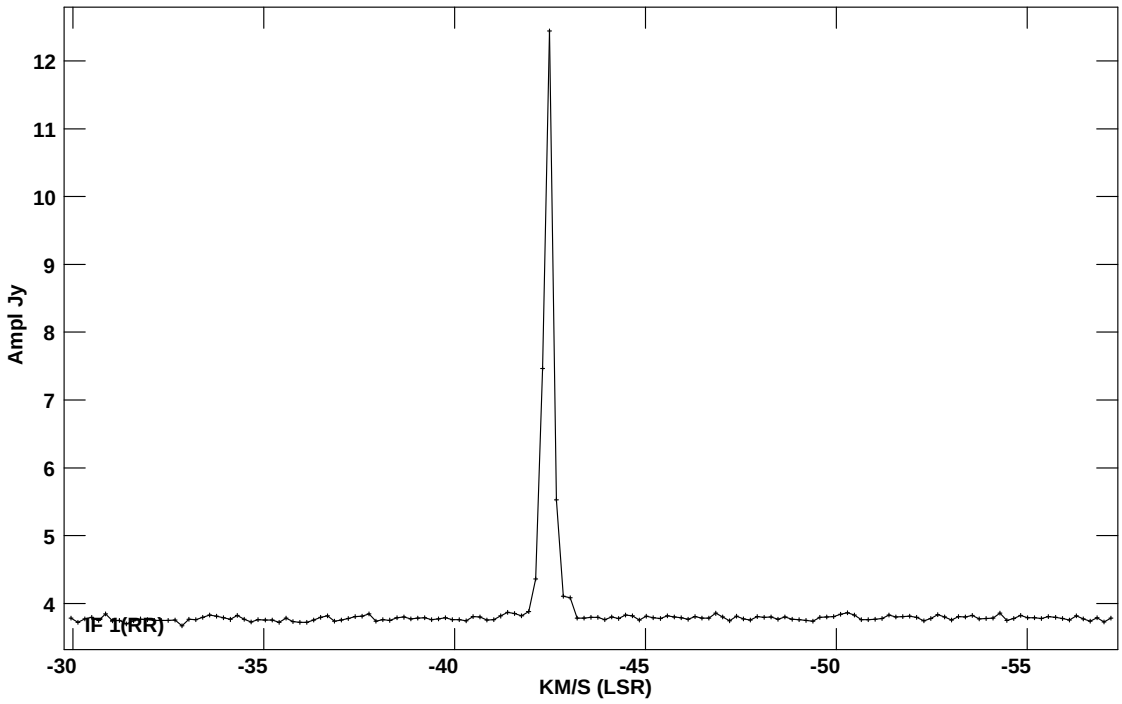

Figure 3.3 MASER detection 1612 MHz W3OH in RR polarization.

The high-mass SFR source W3OH was the only source we observed to have both 1612 and 1720 MHz transitions. The 1612 MHz features are 6.0, 3.1, and 2.5 Janskys above the noise Fig. 3.5. The 1720 MHz MASER emission features are 3.0, 2.2, 1.9, 1.0, and possibly 0.2 Janskys above the noise Fig. 3.6

The high-mass SFR source 98.04+1.45 had 1612 MHz emission 0.2 Janskys above the noise Fig. A.9.

The high-mass SFR source NGC 7538 had 1720 MHz emission 8.5 and 2.4 Janskys above the noise Fig. A.15.

The high-mass SFR source 49.49-0.39 had 1720 MHz emission 35, 24, and 6.0 Janskys above the noise Fig. A.12.

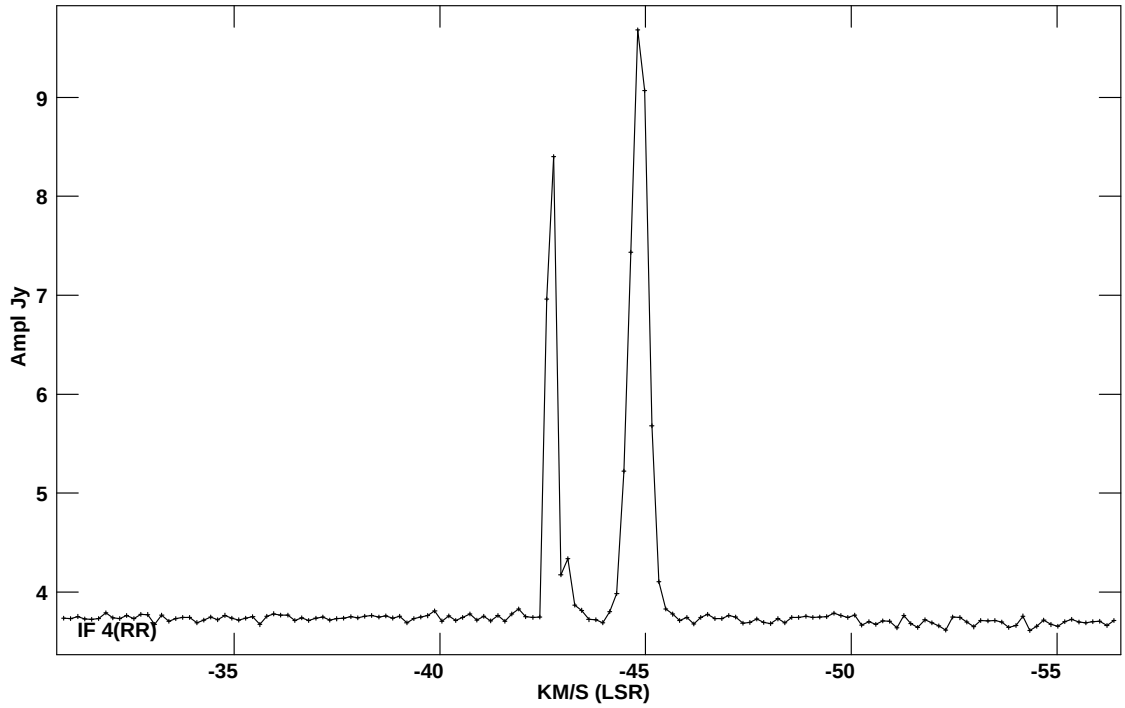

Figure 3.4 MASER detection 1720 MHz W3OH in RR polarization.

The high-mass SFR source 35.20-1.73 had 1720 MHz emission 1 Jansky above the noise Fig. A.8.

The high-mass SFR source W75N had 1720 MHz emission 1.0 and 0.23 Janskys above the noise Fig. A.10.

The high-mass SFR source W75S had 1720 MHz emission 0.35 Janskys above the noise Fig. A.11.

The source 30.60-0.06 had 1612 MHz emission 0.4 Janskys above the noise Fig. A.6.It is not known whether this is a high-mass or low-mass SFR.

The source 20.86+0.48 had 1612 MHz emission 0.6 Janskys above the noise Fig. A.4.It is not known whether this is a high-mass or low-mass SFR.

The source 12.22-0.12 had 1612 MHz emission 0.25 Janskys above the noise Fig. A.1. It is not known whether this is a high-mass or low-mass SFR.

The source 28.87+0.06 had 1720 MHz emission 0.5 Janskys above the noise Fig. A.5.It is not known whether this is a high-mass or low-mass SFR.

The source 12.68-0.18 had 1720 MHz emission 0.49 Janskys above the noise Fig. A.2.It is not known whether this is a high-mass or low-mass SFR.

The source 31.29+0.06 had 1720 MHz emission 0.3 Janskys above the noise Fig. A.7.It is not known whether this is a high-mass or low-mass SFR.

The source 12.91-0.26 had 1720 MHz emission 0.1 Janskys above the noise Fig. A.3.It is not known whether this is a high-mass or low-mass SFR.

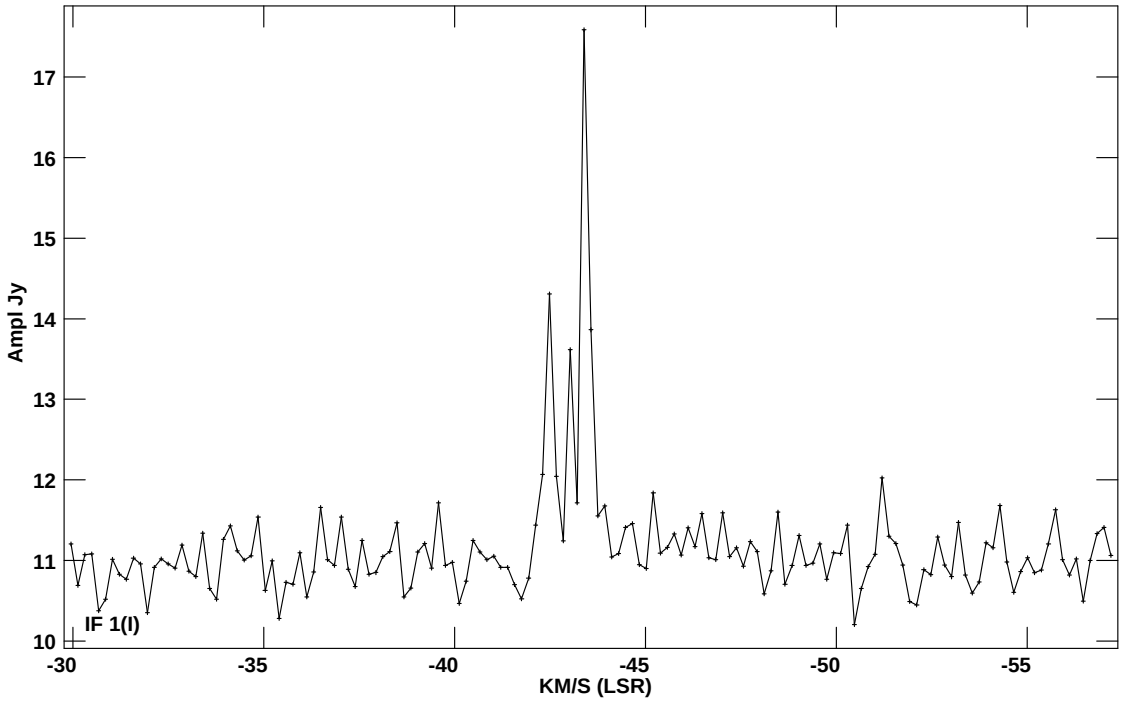

Figure 3.5 MASER detection at 1612 MHz of W3OH. The horizontal axis is the LSR velocity. The vertical axis is in Janskys a unit of intensity

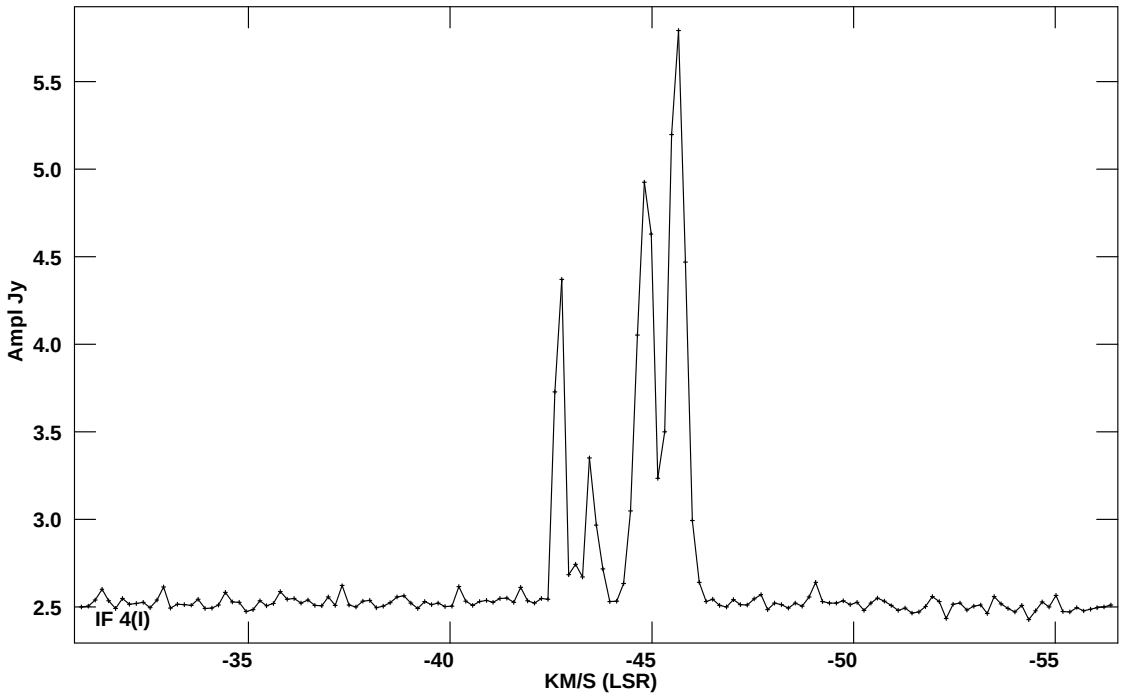

Figure 3.6 MASER detection 1720 MHz W3OH.

Table 3.1 Summary of detections of the strongest OH-MASER emission for the given sources. The common source names and IRAS names are given with galactic coordinates and RA and Dec and V_{LSR}. The symbol † means no detection.

	Galactic	Common	R.A.	DEC	V_{LSR}	Frequency (MHZ)		Mass
IRAS Name	Coordinates	Name	(J2000)	(J2000)	(km/s)	1612	1720	H/L
02232+6138	133.90+1.10	W3(OH)	02 27 04.1	+ 61 52 22	-44.3	6.0 Jy	3.0 Jy	high
21413+5442	98.04+1.45		21 43 00.9	+ 54 56 19	-61.0	0.2 Jy	†	high
23116+6111	111.54+0.78	NGC 7538	23 13 45.3	+ 61 28 10	-57.4	†	8.5 Jy	high
	49.49-0.39	W51	19 23 43.9	+ 14 30 27	57.0	†	35.0 Jy	high
18895+0108	35.20-1.73	W48	19 01 45.5	+ 01 13 32	32.1	†	1.0 Jy	high
	81.87+.078	W75N	20 38 37.5	+ 42 37 54	7.0	†	1.0 Jy	high
	81.72+0.57	W75S	20 39 00.9	+ 42 22 48	1.0	†	0.35 Jy	high
18075-1956	10.62-0.38	W31	18 10 28.6	- 19 55 51	-2.2	†	†	high
18507+0110	34.26+0.15		18 53 18.7	+ 01 14 59	58.0	†	†	high
22543+6145	109.87+2.11	CEPA	22 56 18	+ 62 01 50	-13.8	†	†	high
22176+6303	106.80+5.31	S 140	22 19 18.4	+ 63 18 45	-8.2	†	†	high
21381+5000	94.60-1.81	GL2789	21 40 00.8	+ 50 13 39	-41.0	†	†	high
18018-2426	6.05-1.45	CRL2059	18 04 53.9	- 24 26 41	11.0	†	†	low
18265-1517	16.87-2.16	L379	18 29 24.5	- 15 15 15	16.0	†	†	low
18273+0113	31.58+5.38	SERPENS	18 29 49.7	+ 01 15 20	9.5	†	†	low
20275+4001	78.89+0.71	AFGL2591	20 29 24.9	+ 40 11 21	-8.8	†	†	low
00338+6312	121.30+0.66	L1287	00 36 47.5	+ 63 29 02	-22.8	†	†	low
05137+3919	168.06+0.82	0513+393	05 17 13.3	+ 39 22 14	-21.0	†	†	low
05168+3634	170.66-0.27	0516+365	05 20 16.1	+ 36 37 21	-16.0	†	†	low
06117+1350	196.45-1.68	S269	06 14 37.3	+ 13 49 36	16.0	†	†	low
	20.86+0.48		18 27 25.9	- 10 30 24	50.0	0.6 Jy	†	n/a
03060-0004	30.60-0.06		18 47 19.9	- 02 05 57	37.5	0.4 Jy	†	n/a
01222-0012	12.22-0.12		18 12 44.5	- 18 24 25	27.0	0.25 Jy	†	n/a
02886+0007	28.87+0.06		18 43 48.1	- 03 35 31	103.0	†	0.5 Jy	n/a
	12.68-0.18	W33B	18 13 54.7	- 18 01 46	61.5	†	0.49 Jy	n/a
03129+0007	31.29+0.06		18 48 45.2	- 01 33 12	107.5	†	0.3 Jy	n/a
18117-1753	12.91-0.26		18 14 39.5	- 17 52 00	35.2	†	0.1 Jy	n/a

Table 3.2 Galactic OH-MASER sources with no detections. The common source names are given with coordinates and V $_{LSR}$. The symbol † means no detection.

	Galactic	Common	R.A.	DEC	V_{LSR}	Frequency (MHZ)		Mass
IRAS Name	Coordinates	Name	(J2000)	(J2000)	(km/s)	1612	1720	H/L
03274-0008	32.74-0.07		18 51 21.5	- 00 12 11	32.3	†	†	n/a
17574-2403	5.88-0.39		18 00 34.4	-24 04 04	14.0	†	†	n/a
18032-2032	9.62+0.20		18 06 14.7	- 20 31 31	1.8	†	†	n/a
01190-0014	11.91-0.15		18 12 11.3	-18 41 30	40.5	†	†	n/a
01289+0049	12.89+0.49		18 11 51.3	- 17 31 29	35.0	†	†	n/a
01961-0023	19.61-0.23		18 27 38	- 11 56 36	42.0	†	†	n/a
02008-0013	20.08-0.13		18 28 10	- 11 28 50	46.5	†	†	n/a
03124-0011	31.24-0.11		18 48 12.4	-01 25 48	21.2	†	†	n/a
03140-0026	31.40-0.26		18 49 33	- 01 29 04	85.0	†	†	n/a
03313-0009	33.13-0.09		18 52 07.3	+ 00 08 06	78.5	†	†	n/a
03558-0003	35.58-0.03		18 56 22.5	+ 02 20 27	48.9	†	†	n/a
21306+5539	97.52+3.18		21 32 11.3	+ 55 53 30	-66.5	†	†	n/a
20350+5126	80.87+0.42	W70	20 36 52.6	+41 36 52.6	-8.0	†	†	n/a
20126+4104	78.12+3.63		20 14 26	+ 41 13 32	-4.0	†	†	n/a

Table 3.3 Galactic OH-MASER sources with detections. The common source names are given with coordinates and V $_{LSR}$. The symbol † means no detection.

IRAS	Galactic	Common	R.A.	DEC	1612	1720	Mass
01222-0012	12.22-0.12		18 12 44.5	- 18 24 25	LL	†	
	12.68-0.18	W33B	18 13 54.7	- 18 01 46	†	RR	
18117-1753	12.91-0.26		18 14 39.5	- 17 52 00	†	RR	
	20.86+0.48		18 27 25.9	- 10 30 24	RR/LL	†	
02886+0007	28.87+0.06		18 43 48.1	- 03 35 31	†	RR/LL	
03060-0004	30.60-0.06		18 47 19.9	- 02 05 57	LL	†	
03129+0007	31.29+0.06		18 48 45.2	- 01 33 12	†	RR/LL	
18895+0108	35.20-1.73	W48	19 01 45.5	+ 01 13 32	†	RR/LL	H
21413+5442	98.04+1.45		21 43 00.9	+ 54 56 19	RR/LL	†	H
	81.87+.078	W75N	20 38 37.5	+ 42 37 54	†	RR/LL	H
	81.72+0.57	W75S	20 39 00.9	+ 42 22 48	†	RR/LL	H
	49.49-0.39	W51	19 23 43.9	+ 14 30 27	†	RR*2/LL*2	H
02232+6138	133.90+1.10	W3(OH)	02 27 04.1	+ 61 52 22	RR/LL	RR*2/LL*2	H
23116+6111	111.54+0.78	NGC 7538	23 13 45.3	+ 61 28 10	†	RR*2/LL	H

Chapter 4

Discussion

The intensity of the MASER emission and the resolution of our instruments allowed us to detect many OH-MASERs and resolve many multi-peaked spectra Fig. A.9. Seven of the twelve known high-mass SFR showed 1612 or 1720 MHz emission. Seven regions with detections are not determined as high-mass or low-mass. None of the eight low-mass SFR show 1612 or 1720 MHz emission. That leaves the other 14 sources having no detection and an unknown mass classification. Having only satellite line emission occur in high-mass SFR of the 20 known high-mass/low-mass SFR shows us there is a correlation.

From the data we obtained spectra that we summarized in Table 3.1. The known high-mass SFR regions have strong MASER emission the unknown SFR that have emission are very weak, and the known low-mass SFR have none detected. This may be the greatest understanding we pull from this OH satellite line survey of SFR. Satellite line detection in high-mass SFR may correlate with line strength. Seeing this line strength can depend on the signal to noise ratio we obtain.

Caswell [4] reported 1720 MHz masers are 1/6 as common as 1665 MHz in the southern sky. It is very rare to find a 1720 MHz detection without a 1665 MHz detection. Caswell explains that this could be because only 1720 emission is above the threshold limit. Since our instruments have a limitation on detecting MASER emission we may only see the appearance of satellite lines where they are strong and intense. The strength of the signal depends on the signal to noise ratio proportional to $\sqrt{t}$. We only observed each source for five minutes which doesn't produce a high signal to noise ratio. Because of short integration (observing) times we were limited to make good maps with great UV coverage.

4.1 Future Study

A study of these sources at similar resolution with longer integration time will provide more evidence for our assumption that the satellite lines only appear in SFR. Being able to observe these sources we studied in this survey for longer integration times will yield a higher signal to noise ratio and will most likely yield the appearance of more satellite lines being detected in these regions. Perhaps with equipment that has enough resolution and sensitivity we may discover that the MASER emission strength is directly related to the mass of nearby proto-stars. The exact cause of how MASER conditions are reached in SFR is unknown and can be studied further through detecting MASER emission with high signal to noise ratios.

Chapter 5

Conclusions

We learned the effectiveness of interferometry techniques that can be used to achieve very high spatial resolution. We learned data reduction procedures in AIPS along with debugging calibration problems, strategies to reduce many sources at once, and applying tables to data. These reductions help us understand the conditions that are occurring in SFR. Caswell [4] noted 1720 MHz emission requires higher density, which is true of high-mass vs. low-mass SFR. We need to consider how large that gap is, and does it mean that low-mass SFR are not dense enough to have 1720 MHz emission.

The OH-MASER 1720 MHz line correlates with high-mass SFR. The 1612 MHz line showed a weaker correlation but still, as in the case of the 1720 MHz line, only appeared in sources that are not previously known as low-mass SFR. From this we learn that the OH satellites are a useful tool in describing and identifying high-mass SFR. We understand that high-mass SFR contain different physical conditions that allow for stronger MASER emission of the OH satellite lines.

Bibliography

[1] F. H. Shu, F. C. Adams, and S. Lizano, "Star formation in molecular clouds - Observation and theory," ARAA .

[2] J. L. Caswell, "Star formation: relationship between the maser species," In *Cosmic Masers: From Proto-Stars to Black Holes*, V. Migenes & M. J. Reid, ed., IAU Symposium **206,** 1–+ (2002).

[3] V. L. Fish and M. J. Reid, "Full-Polarization Observations of OH Masers in Massive Star-forming Regions. II. Maser Properties and the Interpretation of Polarization," ApJs **164,** 99–123 (2006).

[4] J. L. Caswell, "OH 1720-MHz masers in southern star-forming regions," MNRAS **349,** 99–114 (2004).

[5] M. J. Reid, A. D. Haschick, B. F. Burke, J. M. Moran, K. J. Johnston, and G. W. Swenson, Jr., "The structure of interstellar hydroxyl masers - VLBI synthesis observations of W3/OH/," ApJ **239,** 89–99 (1980).

[6] A. D. Haschick, M. J. Reid, B. F. Burke, J. M. Moran, and G. Miller, "VLBI aperture synthesis observations of the OH maser source W75 N," ApJ **244,** 76–87 (1981).

[7] X. Zheng, "VLBI observation of OH masers in G 45.07+0.13," Chinese Astronomy and Astrophysics **21,** 182–190 (1997).

[8] V. I. Slysh *et al.*, "Space-VLBI observations of the OH maser OH34.26+0.15: low interstellar scattering," MNRAS **320,** 217–223 (2001).

[9] V. I. Slysh, V. Migenes, I. E. Val'tts, S. Y. Lyubchenko, S. Horiuchi, V. I. Altunin, E. B. Fomalont, and M. Inoue, "Total Linear Polarization in the OH Maser W75 N: VLBA Polarization Structure," ApJ **564,** 317–326 (2002).

[10] M. J. M. Thompson, A. R. and J. Swenson, *Interferometry & Synthesis in Radio Astronomy* (2001).

[11] R. E. Spencer, "Fundamentals of interferometry.," In *Techniques and Applications of Very Long Baseline Interferometry*, pp. 11–25 (1989).

[12] B. Anderson, "Basic radio astronomy.," In *Techniques and Applications of Very Long Baseline Interferometry*, pp. 3–10 (1989).

Appendix A

The list of plots of MASER emission

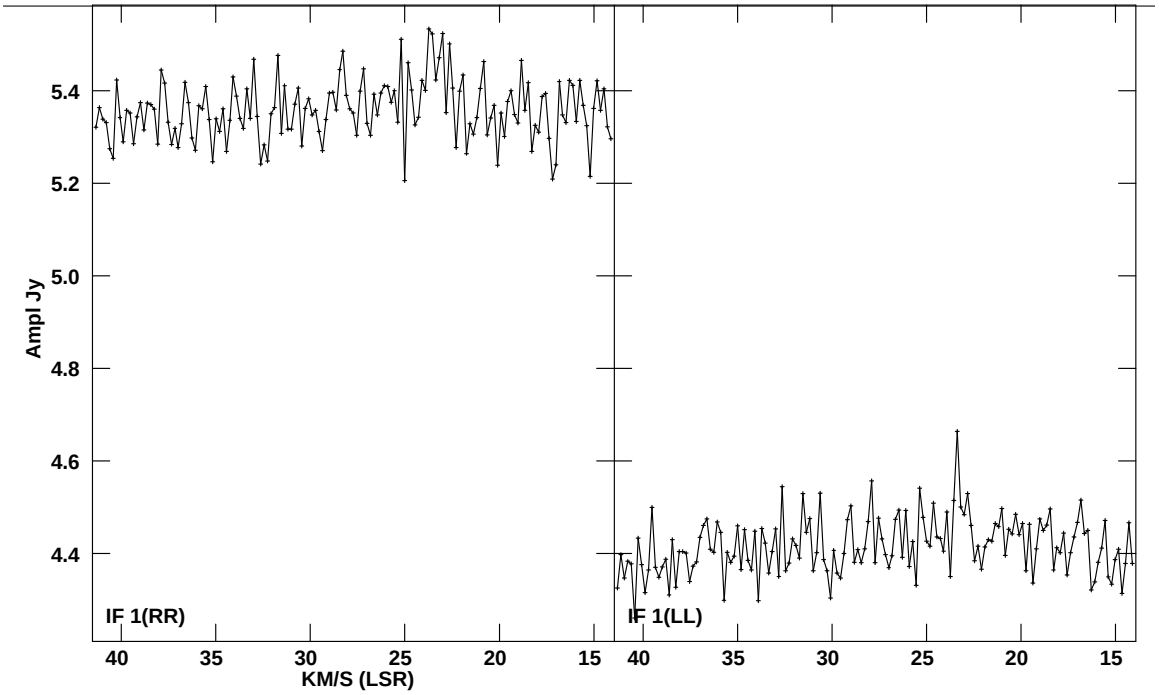

Figure A.1 MASER detection at 1612 MHz of 12.22-0.12.

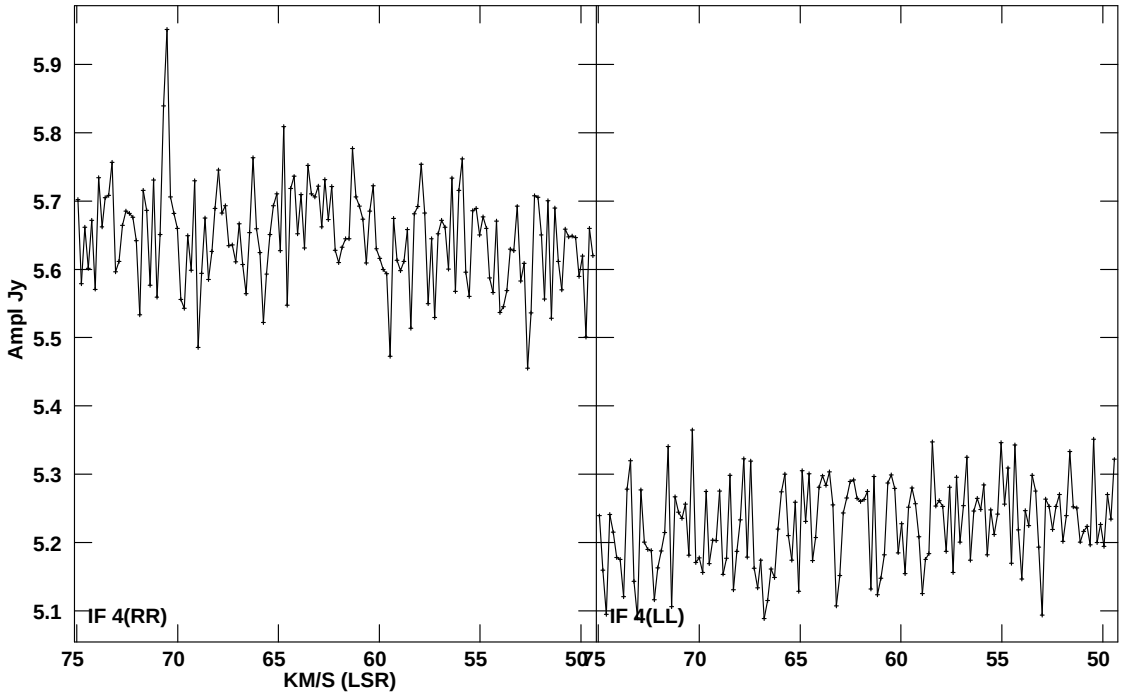

Figure A.2 MASER detection at 1720 MHz of 12.68-0.18.

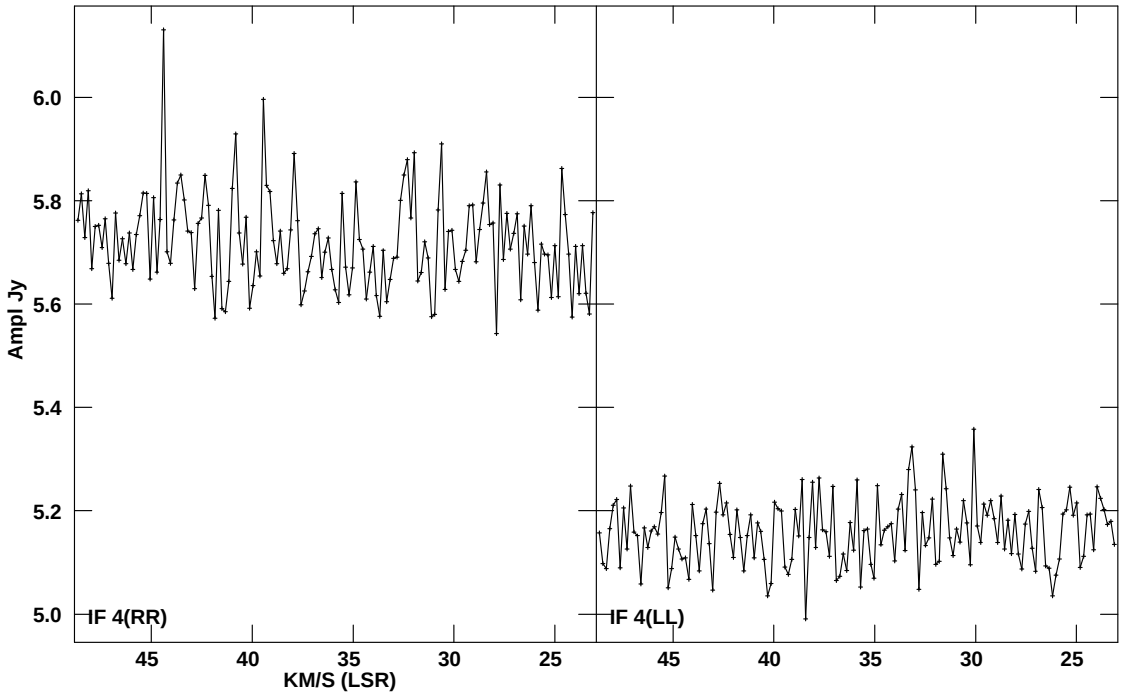

Figure A.3 MASER detection at 1720 MHz of 12.91-0.26.

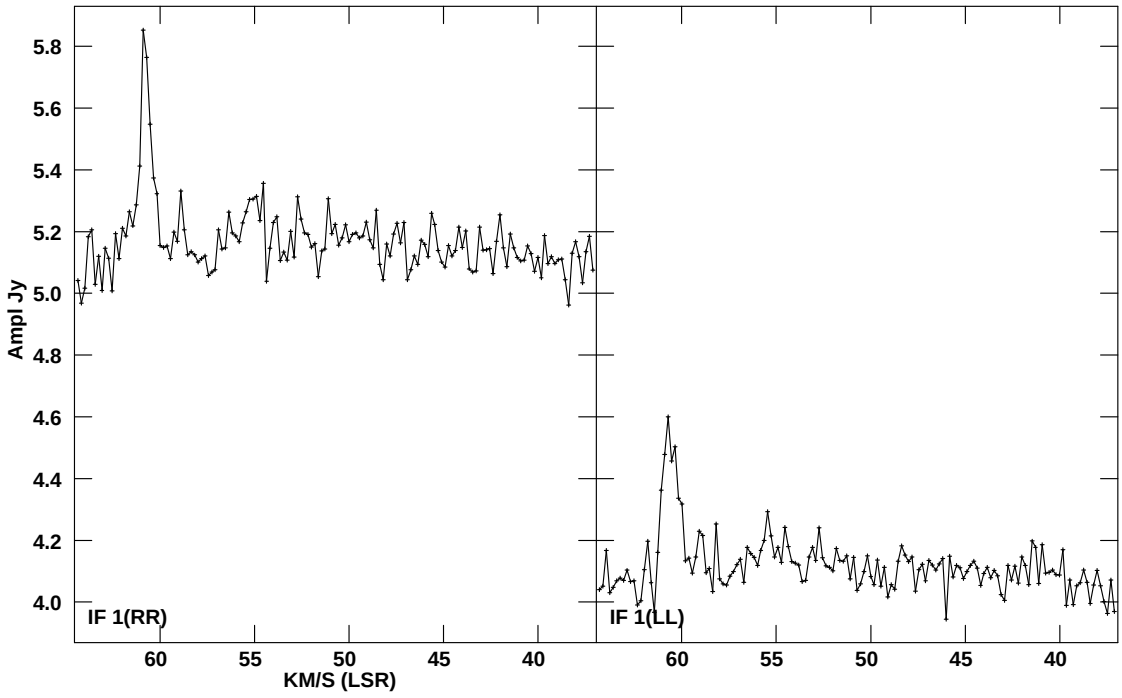

Figure A.4 MASER detection at 1612 MHz of 20.86+0.48.

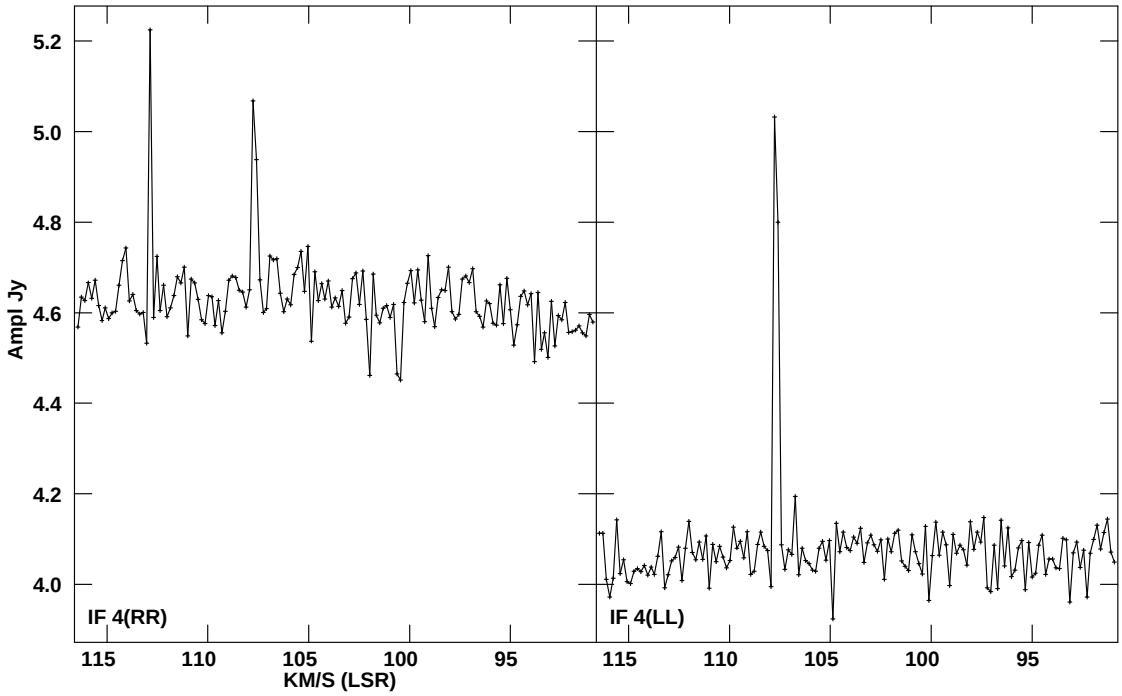

Figure A.5 MASER detection at 1720 MHz of 28.87+0.06.

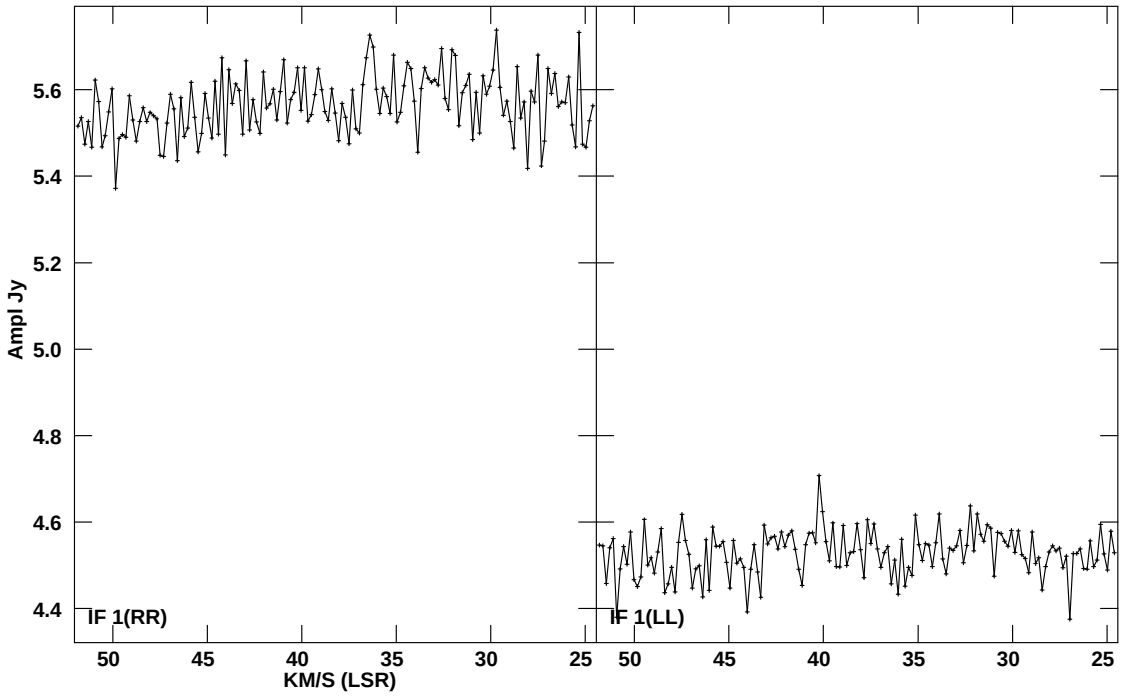

Figure A.6 MASER detection at 1612 MHz of 30.60-0.06.

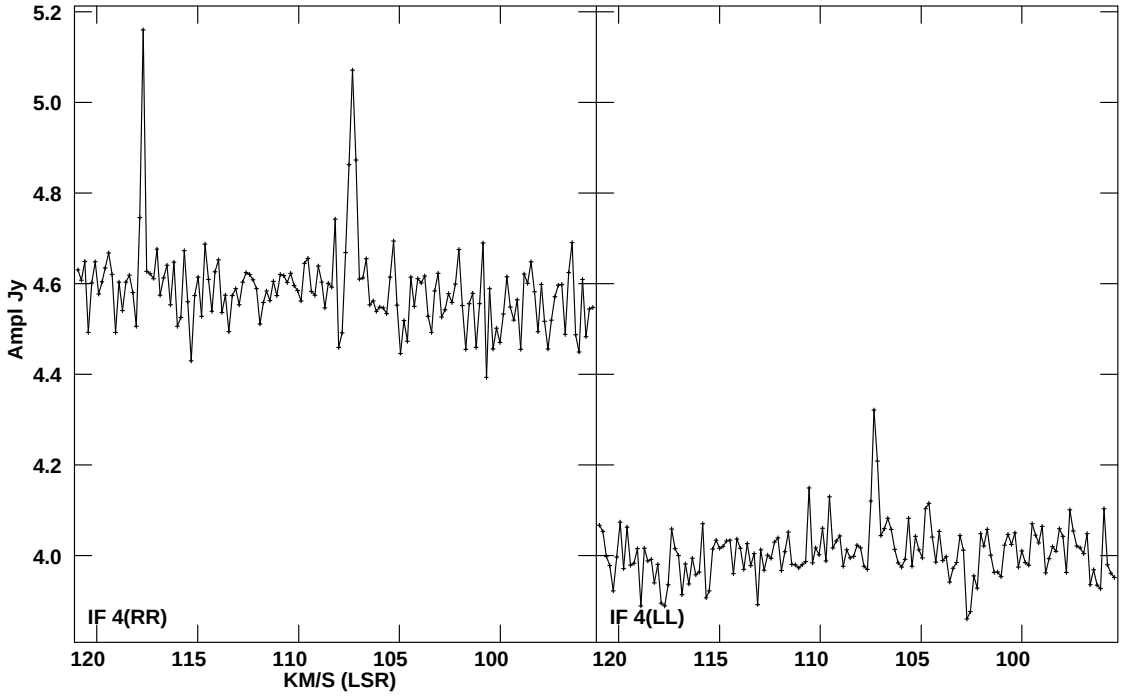

Figure A.7 MASER detection at 1720 MHz of 31.29+0.06.

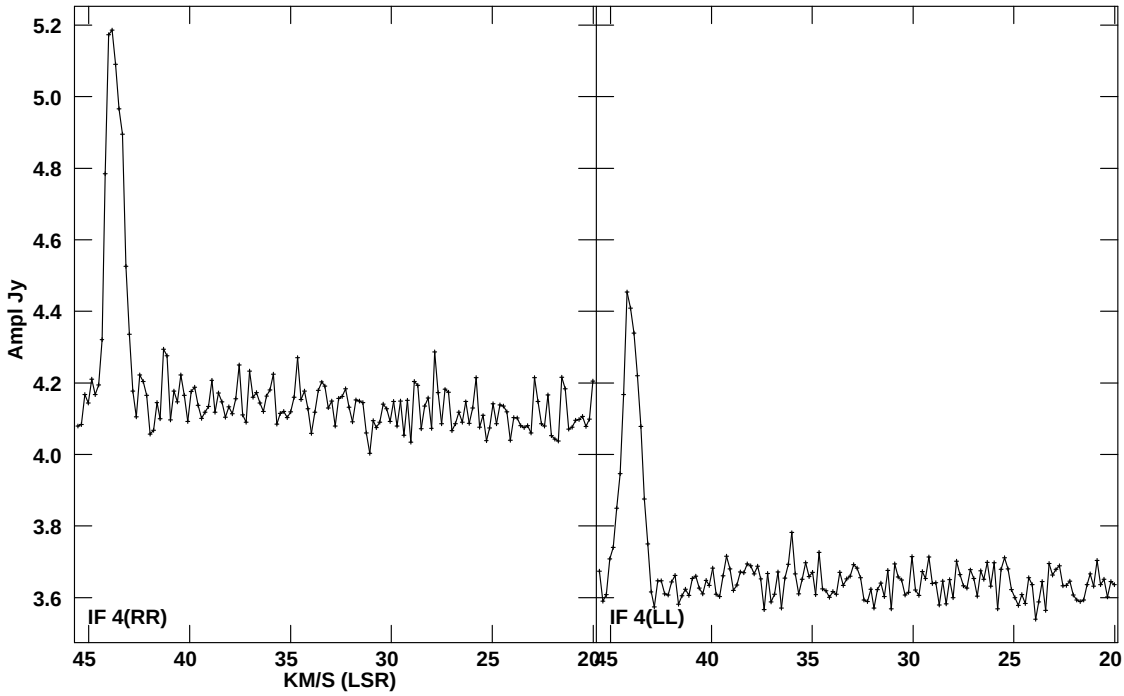

Figure A.8 MASER detection at 1720 MHz of 35.20-1.73.

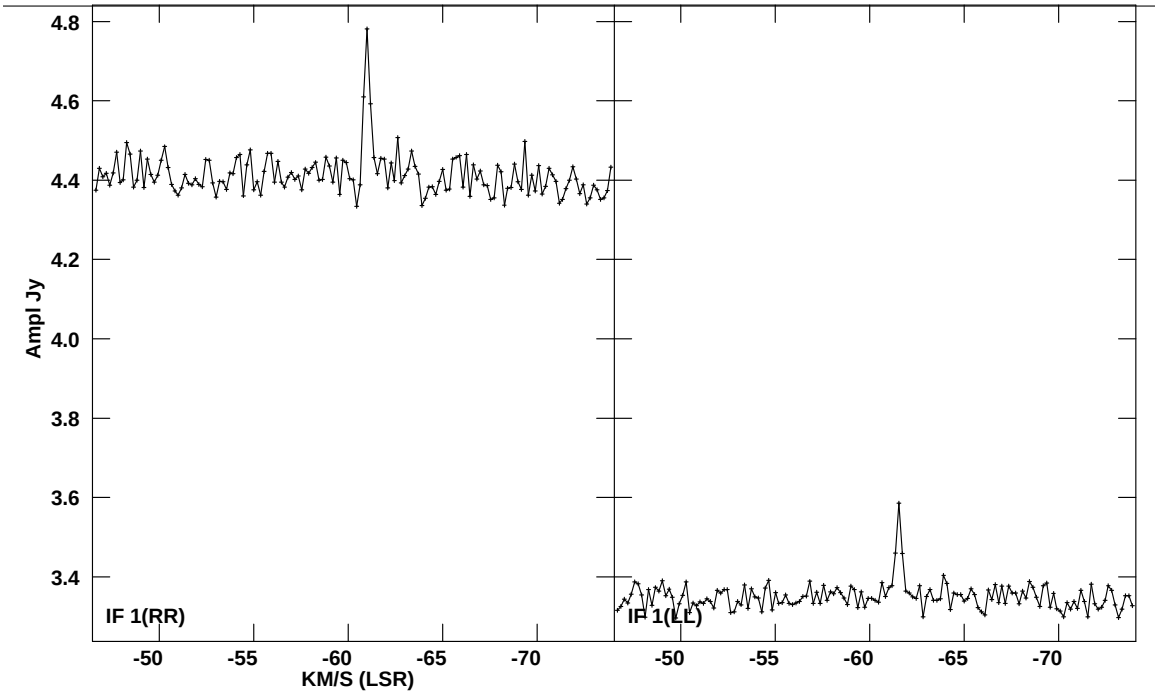

Figure A.9 MASER detection at 1612 MHz of 98.04+1.45.

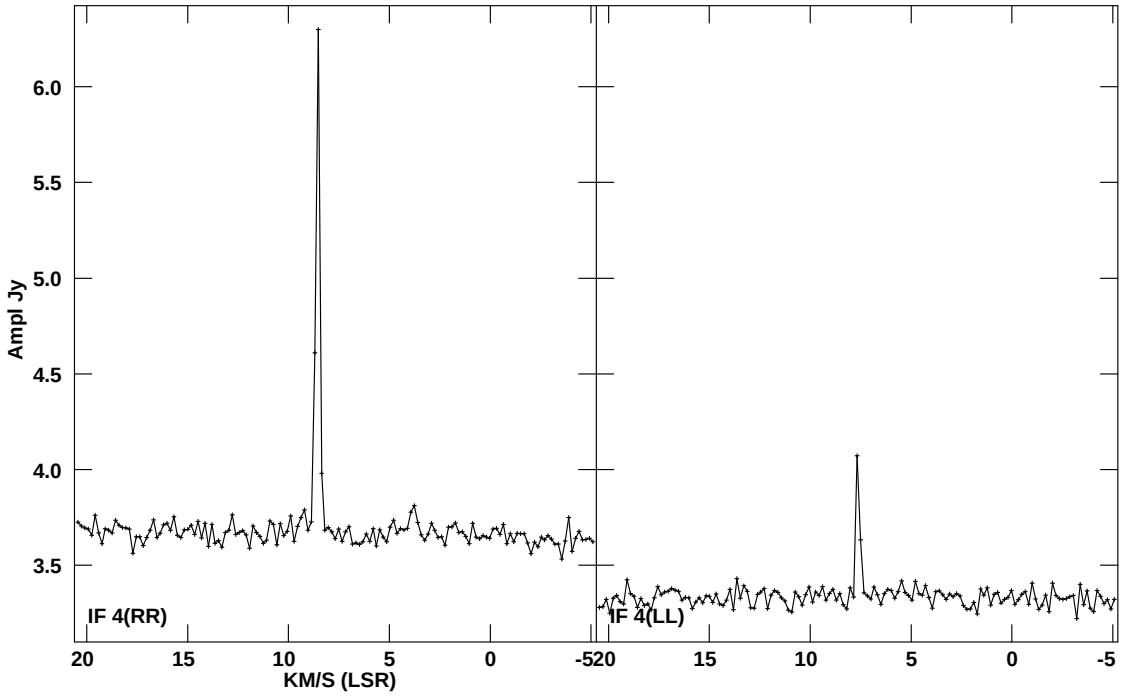

Figure A.10 MASER detection at 1720 MHz of W75N.

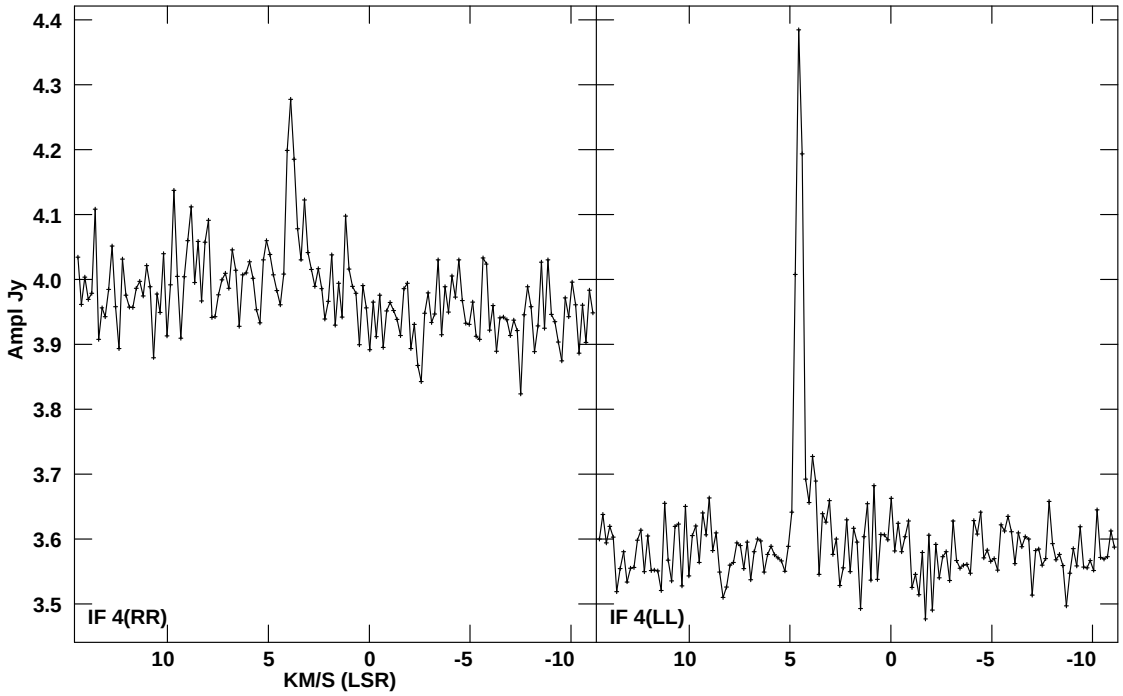

Figure A.11 MASER detection at 1720 MHz of W75S.

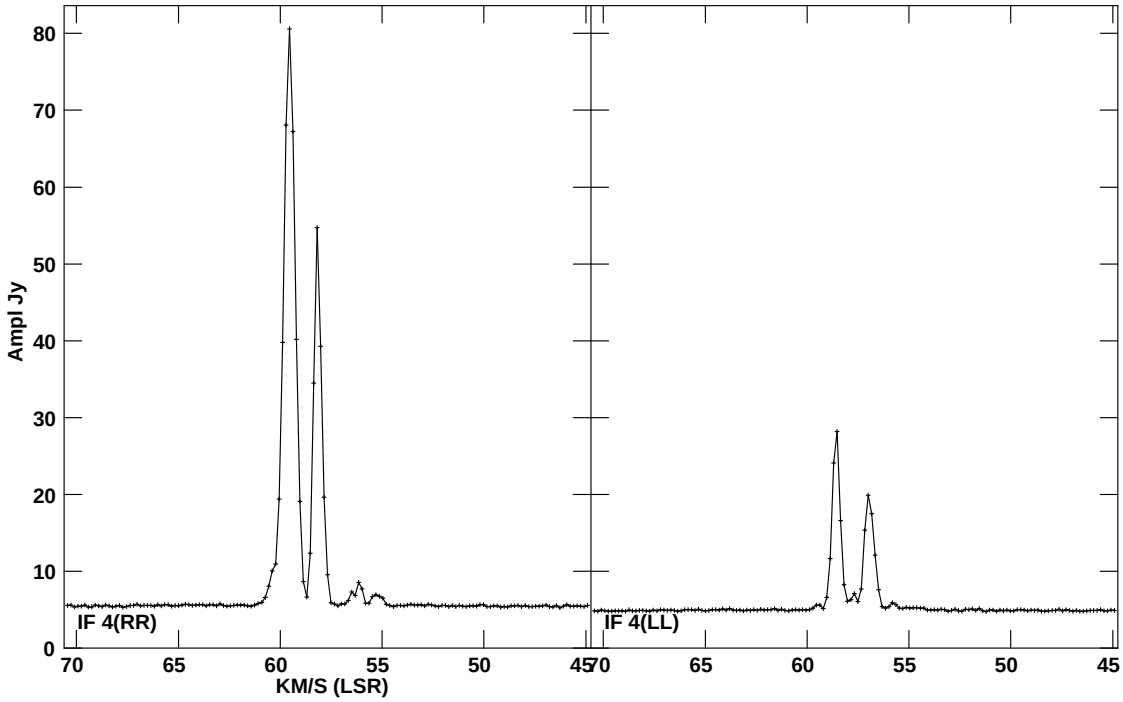

Figure A.12 MASER detection at 1720 MHz of 49.49-0.39.

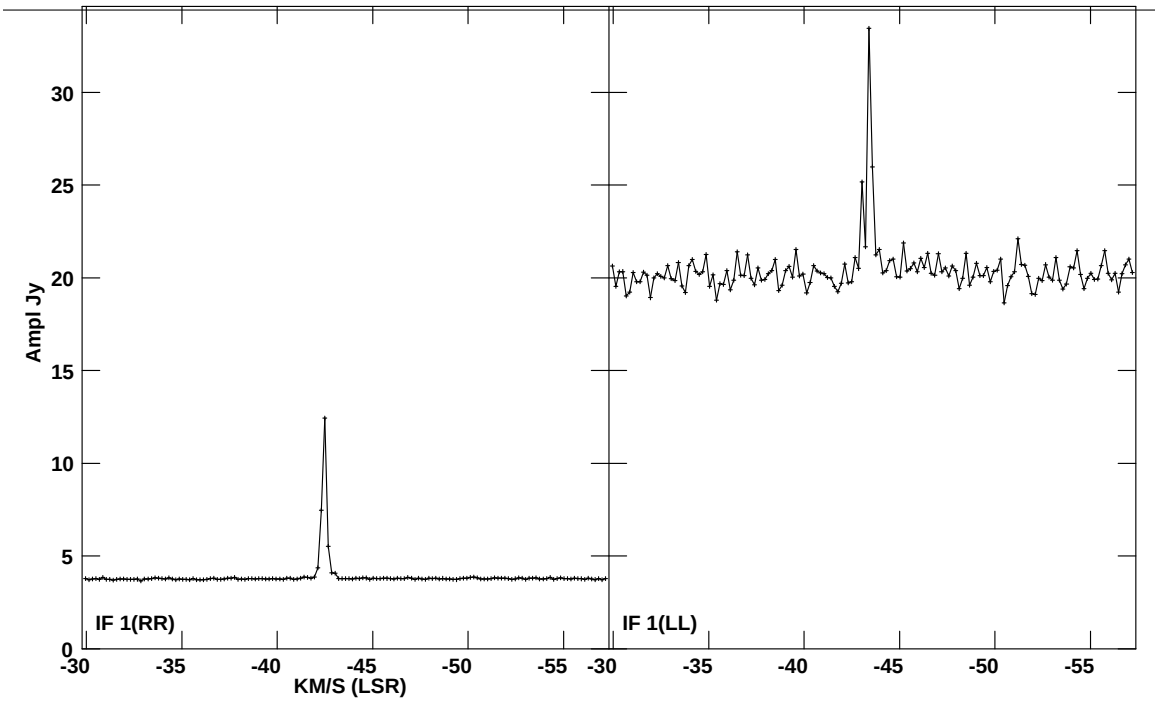

Figure A.13 MASER detection at 1612 MHz of W3OH.

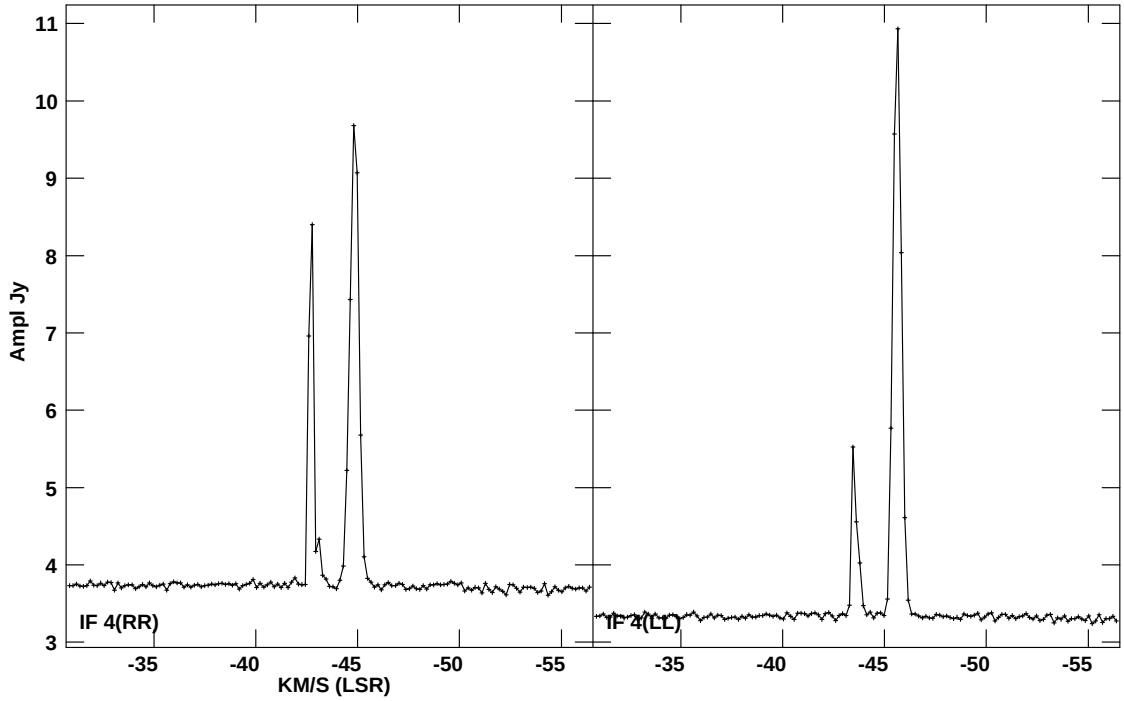

Figure A.14 MASER detection at 1720 MHz of W3OH.

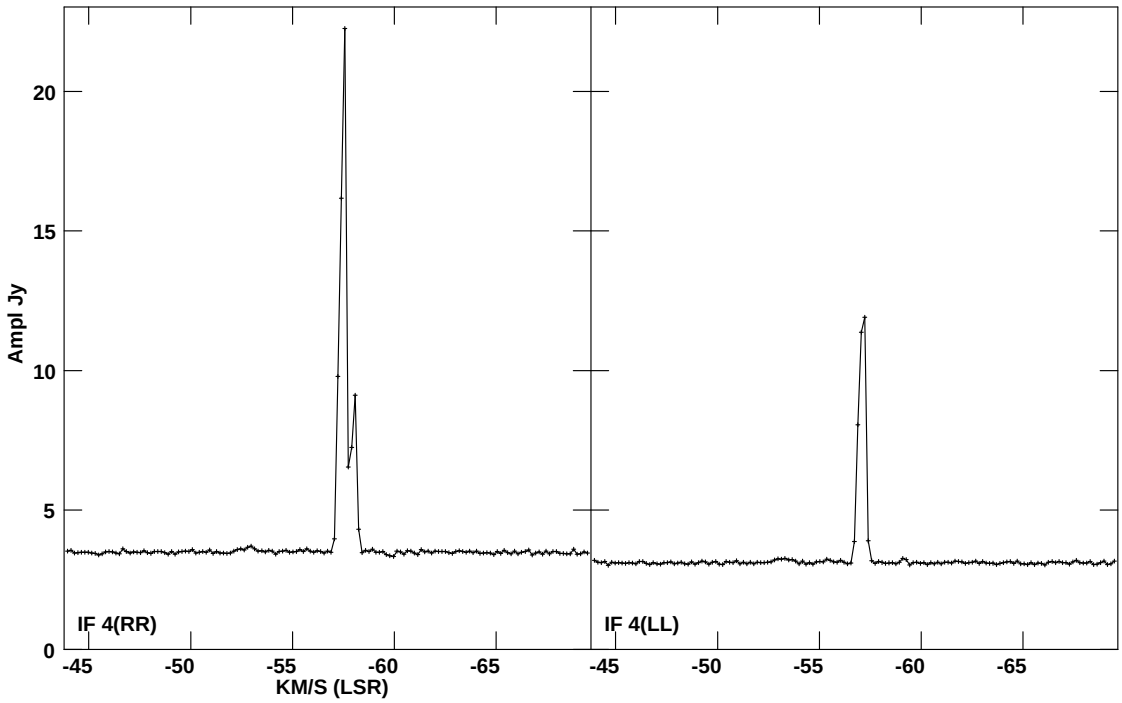

Figure A.15 MASER detection at 1720 MHz of NGC 7538.